

Hydrodynamic mobility of chiral colloidal aggregates

Eric E. Keaveny and Michael J. Shelley

*Applied Mathematics Laboratory, Courant Institute of Mathematical Sciences, New York University, 251 Mercer Street,
New York, New York 10012, USA*

(Received 27 February 2009; published 28 May 2009)

A recent advance in colloidal technology [Zerrouki *et al.*, *Nature (London)* **455**, 380 (2008)] uses magnetic aggregation to enable the formation of micron-scale particle clusters with helical symmetry. The basic building blocks of these aggregates are doublets composed of two micron-scale beads of different radii bonded together by a magnetic cement. Such self-assembled structures offer potential for controllable transport and separation in a low Reynolds number environment using externally applied magnetic or electric fields. Establishing the hydrodynamic properties of the aggregates, in particular the coupling between rotation and translation afforded by the cluster geometry, is an essential initial step toward the design of microfluidic devices employing these aggregates. To quantify this coupling, we first determine parametrized expressions that describe the positions of the beads in an aggregate as a function of size ratio of the two beads composing the doublets. With the geometry of the structure known, we perform hydrodynamic calculations to ascertain entries of the mobility matrix for the aggregate and establish the relationship between the applied torque about the helical axis and translations parallel to this direction. We find that for larger values of the particle radius ratio the coupling between rotations and translations changes sign as the number of doublets in the aggregate increases. This feature indicates that the clusters possess a more complex superhelical structure.

DOI: [10.1103/PhysRevE.79.051405](https://doi.org/10.1103/PhysRevE.79.051405)

PACS number(s): 82.70.-y, 47.57.J-, 47.57.E-, 47.61.-k

I. INTRODUCTION

In recent years, spherical micron-sized paramagnetic beads have been key components in a variety of microfluidic applications. Traditionally, high volume fraction suspensions of such particles have been employed in advanced damping and shock absorbing devices where applied magnetic fields are used to adjust the macroscopic rheological properties of the suspension [1]. Microfluidic devices employing paramagnetic particles rely on the manipulation of the linear self-assembled structures that form in the presence of a uniform applied field [2,3]. In static fields, these linear chains can be used to span a microchannel and filter DNA [4], or when subject to time dependent, rotating fields, pump [5], or mix fluid [6]. Further, the surfaces of the beads can be chemically active allowing them to be flexibly joined together to form magnetically active microfilaments [7,8]. Such filaments have been used previously in a microfluidic mixing device [9], as well as the propulsive tail of an artificial microswimmer [10].

This artificial microswimmer can execute both flagellum-beating [10–12] and corkscrew-type [13] swimming strategies and represents the first step toward controllable biomimetic devices for low Reynolds number transport. More recently, advances in colloidal technology demonstrated that nonspherical magnetic particles can aggregate into functional structures that possess a chiral symmetry [14]. The building block of these clusters is a pair of micron-scale spherical silica beads of different radii that are bonded together with a magnetic cement, which forms a ring around the point where the two beads contact. When subject to an applied magnetic field, the doublets orient their axes perpendicular to the applied field. This is due to the torque the magnetic field exerts on the ringlike distribution of magnetic material binding the beads together. In addition to orienting the particles, the

magnetic field induces a magnetic dipole moment in each bond that leads to doublet-doublet attraction. As the doublets come into contact, asymmetric steric interactions resulting from different bead sizes force the aggregate to take on a helical structure. Like the helical flagellar bundles that *E. Coli* bacteria use to propel themselves [15,16], this geometry affords the coupling of rotation and translation and like the artificial microswimmer, these rotations may be provided by torques generated by externally applied fields. Such clusters may therefore offer unprecedented controllable transport and separation capabilities in a low Reynolds number environment.

The primary focus of this study is to quantify the hydrodynamic properties of these clusters with specific attention paid to the strength and sign of the rotational-translational coupling. To do this, we first determine a geometric relation that relates the positions of the beads in one doublet to its neighbors by finding helical paths that pass through the particle centers. The parameters governing these curves depend exclusively on the size ratio, R , of the two beads comprising a single doublet. This geometric analysis is presented in Sec. II. Having determined the positions of the beads, we employ the force-coupling method (FCM) [17,18] to construct the low Reynolds number mobility matrix for the bead ensemble and calculate entries of the mobility matrix for the aggregate as a whole. These entries are determined as a function of the number of doublets in the aggregate, N_d , as well as the size ratio R . From this analysis, we report that the aggregates have hydrodynamic properties similar to those of superhelices [19] as we find that for large R , the aggregate handedness changes as N_d increases, which in turn affects the direction of transport.

II. CLUSTER GEOMETRY

To determine the hydrodynamic mobility of an aggregate, its geometry must first be established. We derive an expres-

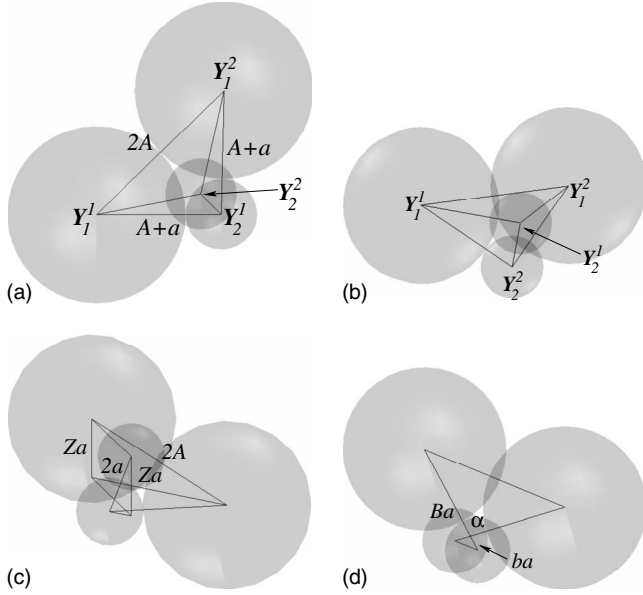


FIG. 1. Images of two doublets in contact. (a) (Top view) and (b) (oblique view) indicate the positions of the beads provided by the hard pack condition, while (c) (oblique view) and (d) (top view) show the parameters that describe the geometry of a cluster.

sion that describes the positions of the beads in an aggregate based on two conditions the doublets must satisfy. The first condition is that neighboring doublets hard pack—each bead of one doublet is in contact with both beads of the neighboring doublet. This condition is sufficient to relate the positions of the beads in one doublet to those of a neighboring doublet. The second condition is that all doublet axes lie in the same plane. This in combination with the first condition establishes the overall geometry of the aggregate.

Consider a doublet, with bead centers \mathbf{Y}_1^1 and \mathbf{Y}_2^1 , aligned with the x axis such that

$$\mathbf{Y}_1^1 = (0, 0, 0), \quad (1)$$

$$\mathbf{Y}_2^1 = (a + A, 0, 0), \quad (2)$$

where the radius of bead 1 is A and the radius of bead 2 is a with $a < A$. In the notation adopted here, the superscript refers to the doublet while the subscript 1 or 2 refers to the large or small particle, respectively. Set the position of the bead of radius A of the neighboring doublet, \mathbf{Y}_1^2 , to lie in the xy plane. Since this sphere is in contact with both particles 1 and 2 of doublet 1, $|\mathbf{Y}_2^2 - \mathbf{Y}_1^1| = 2A$ and $|\mathbf{Y}_1^2 - \mathbf{Y}_2^1| = a + A$. This establishes an isosceles triangle that allows us to determine \mathbf{Y}_1^2 as

$$\mathbf{Y}_1^2 = 2A(\sin \theta, \cos \theta, 0), \quad (3)$$

where 2θ is the magnitude of the angle between the two sides of the triangle of length $a + A$ [see Fig. 1(a)]. A similar geometric argument can be made to determine the position of \mathbf{Y}_2^2 [Fig. 1(b)] as

$$\begin{aligned} \mathbf{Y}_2^2 = & A(\sin \theta, \cos \theta, 0) \\ & + C(\cos \phi \cos \theta, -\cos \phi \sin \theta, -\sin \phi), \end{aligned} \quad (4)$$

where $C^2 = (a + A)^2 - A^2$ and $\sin(\phi/2) = a/C$. To ensure right-handed symmetry of the emerging helix, the z component of \mathbf{Y}_2^2 is chosen to be negative.

While the first condition allowed us to relate the position and orientation of one doublet to its neighbor, a second condition is needed to establish an axis of symmetry and provide the geometry of the entire aggregate. If we introduce a third doublet to be in contact with doublet 2, we find that there is a range of positions for \mathbf{Y}_1^3 and \mathbf{Y}_2^3 that satisfy the first condition. The two extremes in this range occur when $|\mathbf{Y}_1^3 - \mathbf{Y}_2^1| = a + A$ and $|\mathbf{Y}_2^3 - \mathbf{Y}_1^1| = a + A$. A second condition, therefore, is needed to eliminate this degree of freedom and provide unique values of \mathbf{Y}_1^3 and \mathbf{Y}_2^3 . Here, we require that each doublet axis, \mathbf{p}_{n_d} , for $n_d = 1, \dots, N_d$, be perpendicular to the applied field \mathbf{H}_0 that induces the formation of the cluster. This condition is based on the approximation that the dipole moment of each magnetic ring is induced by and responds to the field \mathbf{H}_0 alone. Thus the magnetic dipole moment [20] for each doublet $n_d = 1, \dots, N_d$, is

$$\mathbf{m}_{n_d} = [K_\alpha \mathbf{p}_{n_d} \mathbf{p}_{n_d} + K_\beta (\mathbf{I} - \mathbf{p}_{n_d} \mathbf{p}_{n_d})] \mathbf{H}_0, \quad (5)$$

where K_α and K_β are constants that depend on the geometry and magnetic susceptibility of the magnetic ring. As the magnetic torque is then given by [21]

$$\boldsymbol{\tau}_{n_d}^{mag} = \mu_0 \mathbf{m}_{n_d} \times \mathbf{H}_0, \quad (6)$$

where μ_0 is the permeability of free space, each doublet will align such that $\mathbf{p}_{n_d} \cdot \mathbf{H}_0 = 0$ for all n_d . As a result, the aggregate's helical axis will coincide with the direction of the applied field as well as the vector $\mathbf{p}_{n_d} \times \mathbf{p}_{n_d+1}$.

With the aggregate's axis thus determined, we may describe the positions of the beads in the aggregate by two simple helical curves. One curve passes through the centers of the larger beads, while the other curve marks the positions of the smaller beads. If we now consider a coordinate system where the helical axis is the z axis and the positions of the beads forming doublet n_d are centered at $\mathbf{Y}_1^{n_d} = a(B, 0, 0)$ and $\mathbf{Y}_2^{n_d} = a(-b, 0, 0)$, where Ba and ba are the distances from the axis for the large and small beads, respectively, the positions of the beads in the neighboring doublet $n_d + 1$ may be written as $\mathbf{Y}_1^{n_d+1} = a(B \cos \alpha, B \sin \alpha, Z)$ and $\mathbf{Y}_2^{n_d+1} = a(-b \cos \alpha, -b \sin \alpha, Z)$ [see Figs. 1(c) and 1(d)]. Similarly, we may write the positions of the beads in doublet $n_d + 2$ as $\mathbf{Y}_1^{n_d+2} = a(B \cos 2\alpha, B \sin 2\alpha, 2Z)$, $\mathbf{Y}_2^{n_d+2} = a(-b \cos 2\alpha, -b \sin 2\alpha, 2Z)$, and so on. Using the four bead positions described earlier, (1)–(4), and also that $(\mathbf{Y}_2^1 - \mathbf{Y}_1^1) \times (\mathbf{Y}_2^2 - \mathbf{Y}_1^2)$ coincides with the helical axis of the aggregate, the dimensionless parameters Z , B , b , and α can be expressed in terms of the particle size ratio $R = A/a \geq 1$. Specifically, these relations are

$$Z = 2R \left(\frac{(1+R)^2 - R^2}{(1+R^2)(2R+1)} \right)^{1/2}, \quad (7)$$

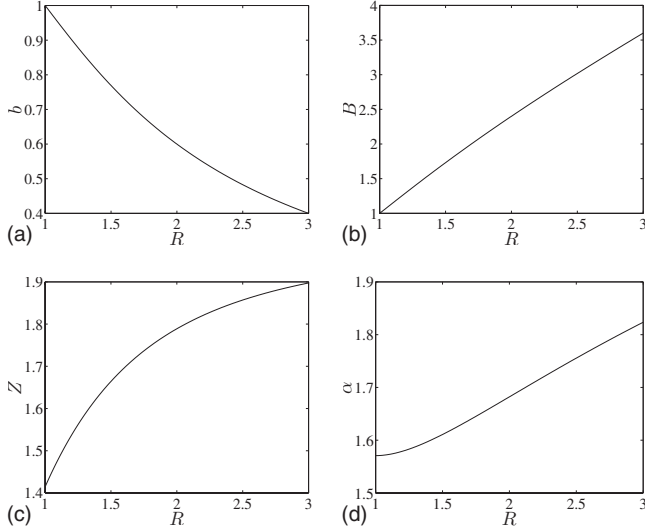


FIG. 2. Geometric parameters (a) b , (b) B , (c) Z , and (d) α as a function of R .

$$b = \frac{1}{1+R^2}(1+R), \quad (8)$$

$$B = \frac{R^2}{1+R^2}(1+R), \quad (9)$$

$$\alpha = 2 \sin^{-1} \left(\frac{\sqrt{1+R^2}}{1+R} \right). \quad (10)$$

The dependence of these expressions on the particle size ratio R is shown in Fig. 2. With these parameters, the equations for the simple helices passing through the centers of the large and small beads of the aggregates as a function of the dimensionless distance along the helical axis, z , are

$$\mathbf{r}(z) = a[b \cos(\alpha z/Z), b \sin(\alpha z/Z), z], \quad (11)$$

$$\mathbf{R}(z) = a[B \cos(\alpha z/Z), B \sin(\alpha z/Z), z]. \quad (12)$$

These equations describe right-handed helices with a pitch $P/a = 2\pi Z/\alpha$. Left-handedness can be achieved by substituting $\alpha \rightarrow -\alpha$. Note that these equations hold for the case where $R=1.0$ even though the aggregate does not exhibit chiral symmetry. Figure 3 shows images of the resulting structure over the range of particle size ratios $1.0 \leq R \leq 3.0$. In the case where $R=1.0$ we see the doublets are oriented perpendicular to each other as observed in the experiments. As the ratio is increased, the emerging helix can be readily observed. The value $R=3.0$ is near an upper limit for particle ratios that allow aggregates to have this geometry. Above this upper limit, the pitch of the helix is not large enough to accommodate the increasingly larger particles. At this maximum value of R , the large bead of doublet n_d+3 is in contact with that of doublet n_d and, accordingly, $|\mathbf{Y}_{n_d+3} - \mathbf{Y}_{n_d}| = 2A$. Therefore, the solution to

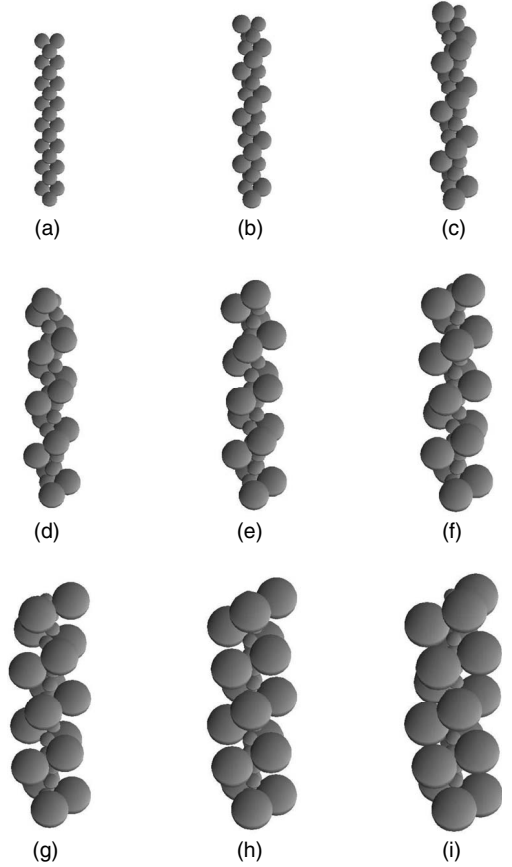


FIG. 3. Images of the aggregates where the positions of the beads have been determined from Eqs. (11) and (12) wherein (a) $R=1.0$, (b) $R=1.25$, (c) $R=1.5$, (d) $R=1.75$, (e) $R=2.0$, (f) $R=2.25$, (g) $R=2.5$, (h) $R=2.75$, and (i) $R=3.0$.

$$4R^2 - 9Z^2 - 2B^2(1 - \cos 3\alpha) = 0 \quad (13)$$

provides the maximum value of R . After substituting the expressions for Z , B , and α and rearranging terms, we obtain a seventh-order equation for R ,

$$2R^7 - 5R^6 - 11R^4 - 6R^3 - 7R^2 - 4R - 1 = 0. \quad (14)$$

Solving this equation numerically, we determine the maximum value as $R \approx 3.1787$ which is the only noncomplex root to Eq. (14). Zerrouki *et al.* [14] also reported a lower limit of $R \approx 2.0$ based on magnetic energy considerations. Since $1.0 \leq R < 3.18$ are geometrically admissible, we will consider particle ratios in this range in our hydrodynamic calculations.

III. CLUSTER MOBILITY

With the geometry now established, we perform calculations to determine the low Reynolds number hydrodynamic mobility of the aggregate. In the context of low Re , translations parallel to and rotations about the helical axis are linearly related to external forces and torques in these respective directions through

$$\begin{bmatrix} U_{\parallel} \\ \Omega_{\parallel} \end{bmatrix} = \begin{bmatrix} M_A & M_B \\ M_B & M_D \end{bmatrix} \begin{bmatrix} F_{\parallel} \\ \tau_{\parallel} \end{bmatrix}. \quad (15)$$

The values of the scalar mobility matrix entries M_A , M_B , and M_D will depend linearly on the viscosity of the fluid, η , but nonlinearly on the geometry of the cluster. Recall that the parameters governing cluster geometry are the size ratio of the beads within each doublet, R , and the number of doublets comprising the cluster, N_d . The value of M_B is of particular importance as this entry provides the strength of the coupling between the torque and translational velocity. Additionally, the sign of M_B indicates the direction the aggregate rotates (clockwise or counterclockwise) if subject to external force parallel to the cluster's axis.

To obtain estimates of M_A , M_B , and M_D for different R and N_d , we employ the FCM [17,18] to construct an approximate mobility matrix for the ensemble of $N=2N_d$ spherical particles. In FCM, each particle n is represented as a finite-force multipole expansion in the Stokes equations truncated at the force dipole,

$$\nabla p - \eta \nabla^2 \mathbf{u} = \sum_{n=1}^N \mathbf{F}^n \Delta_n(\mathbf{x} - \mathbf{Y}_n) + \mathbf{G}^n \cdot \nabla \Xi_n(\mathbf{x} - \mathbf{Y}_n), \quad (16)$$

$$\nabla \cdot \mathbf{u} = 0, \quad (17)$$

where

$$\Delta_n(\mathbf{x}) = (2\pi\sigma_{n,\Delta}^2)^{-3/2} e^{-r^2/2\sigma_{n,\Delta}^2}, \quad (18)$$

$$\Xi_n(\mathbf{x}) = (2\pi\sigma_{n,\Xi}^2)^{-3/2} e^{-r^2/2\sigma_{n,\Xi}^2}. \quad (19)$$

The length scales $\sigma_{n,\Delta}$ and $\sigma_{n,\Xi}$ are related to the radius of bead n , a_n through $a_n = \sqrt{\pi}\sigma_{n,\Delta} = (6\sqrt{\pi})^{1/3}\sigma_{n,\Xi}$. In Eq. (16), \mathbf{F}^n is the total external force on bead n ; the antisymmetric part of the tensor \mathbf{G}^n is related to the torque on the bead τ^n through $(G_{ij}^n - G_{ji}^n)/2 = \frac{1}{2}\epsilon_{ijk}\tau_k^n$ and the symmetric part is chosen so that

$$\int \frac{1}{2} [\nabla \mathbf{u} + (\nabla \mathbf{u})^T] \Xi_n(\mathbf{x} - \mathbf{Y}_n) d^3 \mathbf{x} = 0. \quad (20)$$

The resulting flow field can be determined exactly and is given in indicial notation by

$$u_i = \sum_{n=1}^N u_i^n(\mathbf{x}) = \sum_{n=1}^N P_{ij}^n(\mathbf{x} - \mathbf{Y}_n) F_j^n + R_{ijk}^n(\mathbf{x} - \mathbf{Y}_n) G_{jk}^n, \quad (21)$$

where

$$P_{ij}^n(\mathbf{x}) = f(r; \sigma_{n,\Delta}) \delta_{ij} + g(r; \sigma_{n,\Delta}) x_i x_j, \quad (22)$$

$$R_{ijk}^n(\mathbf{x}) = \frac{df(r; \sigma_{n,\Xi})}{dr} x_k \delta_{ij} / r + g(r; \sigma_{n,\Xi}) (\delta_{ik} x_j + \delta_{jk} x_i) + \frac{dg(r; \sigma_{n,\Xi})}{dr} x_i x_j x_k / r, \quad (23)$$

with

$$f(r; \sigma) = \frac{1}{8\pi\eta r} \left[\left(1 + \frac{\sigma^2}{r^2} \right) \operatorname{erf} \left(\frac{r}{\sigma\sqrt{2}} \right) - \frac{2\sigma}{r\sqrt{2\pi}} e^{-r^2/(2\sigma^2)} \right], \quad (24)$$

$$g(r; \sigma) = \frac{1}{8\pi\eta r^3} \left[\left(1 - \frac{3\sigma^2}{r^2} \right) \operatorname{erf} \left(\frac{r}{\sigma\sqrt{2}} \right) + \frac{6\sigma}{r\sqrt{2\pi}} e^{-r^2/(2\sigma^2)} \right], \quad (25)$$

and $r = |\mathbf{x}|$. FCM solutions (22) and (23) are asymptotic to the Stokeslet, rotlet, and stresslet fundamental solutions and provide the corresponding degenerate multipoles associated with these terms. The velocity and angular velocity of each bead n are then determined from the resulting flow field as

$$\mathbf{V}_n = \int \mathbf{u}(\mathbf{x}) \Delta_n(\mathbf{x} - \mathbf{Y}_n) d^3 \mathbf{x}, \quad (26)$$

$$\Omega_n = \frac{1}{2} \int \boldsymbol{\omega}(\mathbf{x}) \Xi_n(\mathbf{x} - \mathbf{Y}_n) d^3 \mathbf{x}, \quad (27)$$

where $\boldsymbol{\omega}$ is the vorticity of the fluid. This volume averaged integration captures the Faxén corrections for particle motion in a spatially varying flow field. The primary limitation of this approach is that FCM does not resolve near-contact lubrication forces. In an aggregate, however, the relative motion of neighboring doublets is limited as a result of the interdoublet magnetic forces. We, therefore, expect lubrication forces to have a minimal effect on the overall dynamics of the cluster.

Using Eqs. (22) and (23) in conjunction with Eqs. (26) and (27), we may perform pairwise calculations to construct the mobility matrices for the collection of spheres comprising the aggregate. These matrices relate moments of the forces on the beads to moments of the fluid velocity at the bead centers and take the form of an $11N \times 11N$ linear system of equations,

$$\begin{bmatrix} \mathcal{V} \\ \mathcal{W} \\ \mathbf{0} \end{bmatrix} = \begin{bmatrix} \mathcal{M}^{VF} & \mathcal{M}^{V\tau} & \mathcal{M}^{VG} \\ \mathcal{M}^{\Omega F} & \mathcal{M}^{\Omega\tau} & \mathcal{M}^{\Omega G} \\ \mathcal{M}^{EF} & \mathcal{M}^{E\tau} & \mathcal{M}^{EG} \end{bmatrix} \begin{bmatrix} \mathcal{F} \\ \mathcal{T} \\ \mathcal{G} \end{bmatrix}. \quad (28)$$

Here, \mathcal{V} and \mathcal{W} are $3N \times 1$ vectors containing the velocity and angular velocity information of all N beads, respectively, and the vector of zeros, $\mathbf{0}$, has dimension $5N \times 1$. On the right-hand side of Eq. (28), \mathcal{F} and \mathcal{T} are $3N \times 1$ vectors that hold all components of the total force and torque on the beads, while \mathcal{G} has dimension $5N \times 1$ and holds the independent components of the beads' stresslets.

By considering two rigid body motions for a given ensemble of beads, we can determine the values of M_A , M_B , and M_D for the aggregate as a whole. We first examine the case where the aggregate is translating in the positive z direction without rotating. Therefore, the motion of each bead n is $V_x^n = V_y^n = 0$, $V_z^n = 1.0$, and $\Omega_x^n = \Omega_y^n = \Omega_z^n = 0$. With these values of the velocities and angular velocities, we solve linear system (28) to obtain the forces and torques on each bead from which we calculate the total force in the z direction $F_{\parallel}^1 = \sum_n F_z^n$ and total torque about the axis $\tau_{\parallel}^1 = \sum_n \tau_z^n + (Y_x^n F_y^n$

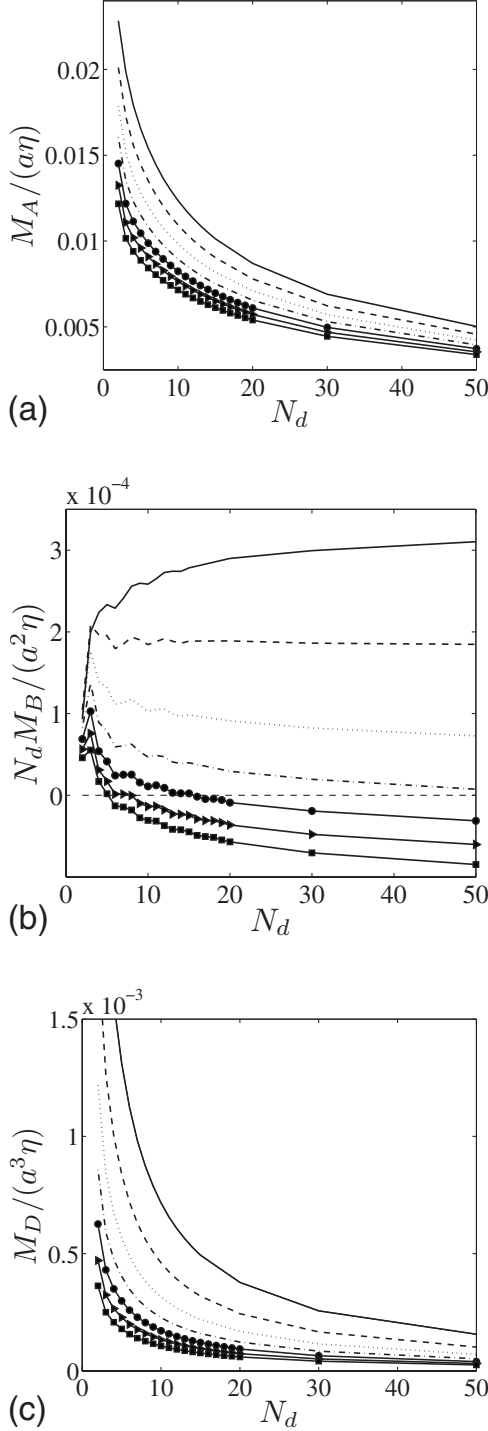


FIG. 4. Entries of the mobility matrix: (a) M_A , (b) $M_B N_d$, and (c) M_D as a function of N_d . In the plots, the solid line corresponds to $R=1.5$, the dashed line corresponds to $R=1.75$, the dotted line corresponds to $R=2.0$, the dashed-dotted line corresponds to $R=2.25$, the solid line with circular markers corresponds to $R=2.5$, the solid line with triangular markers corresponds to $R=2.75$, and the solid line with square markers corresponds to $R=3.0$.

$-Y_y^n F_x^n$). We perform the same calculation for the second rigid body motion where the aggregate rotates without translating. In this case, the beads' motions are given by $V_x^n = -Y_y^n$, $V_y^n = Y_x^n$, and $V_z^n = 0$ and $\Omega_x^n = \Omega_y^n = 0$ and $\Omega_z^n = 1$ and

we again solve Eq. (28) to determine the total force and torque, F_{\parallel}^2 and τ_{\parallel}^2 , respectively. With the total forces and torques for these two cases known, we may determine the entries M_A , M_B , and M_D for the aggregate from Eq. (15) rewritten as

$$\begin{bmatrix} 1 \\ 0 \\ 1 \\ 0 \end{bmatrix} = \begin{bmatrix} F_{\parallel}^1 & \tau_{\parallel}^1 & 0 & 0 \\ F_{\parallel}^2 & \tau_{\parallel}^2 & 0 & 0 \\ 0 & 0 & F_{\parallel}^2 & \tau_{\parallel}^2 \\ 0 & 0 & F_{\parallel}^1 & \tau_{\parallel}^1 \end{bmatrix} \begin{bmatrix} M_A \\ M_B \\ M_B \\ M_D \end{bmatrix}. \quad (29)$$

Figure 4 shows the values of M_A , $M_B N_d$, and M_D as a function of N_d for various values of R . We multiplied M_B by N_d since the magnetic torques used to manipulate an aggregate in an experimental setting will increase linearly with N_d . The value plotted, therefore, indicates how the velocity of an actuated aggregate will change as N_d increases. As expected, M_A and M_D are found to decrease uniformly with both N_d and R as these parameters indicate an overall increase in the size of the object. The dependence of M_B on these parameters demonstrates the interesting hydrodynamic properties of these aggregates. We find that for larger R , the sign of M_B will depend on N_d . Specifically, an aggregate whose geometry can be described by Eqs. (11) and (12) with $\alpha > 0$ will translate in the positive z direction when N_d is low and $\tau_{\parallel} > 0$. However, at higher values of N_d , this aggregate will move in the negative z direction.

This kind of behavior has previously been observed before with superhelices [19]—helices whose axes are themselves helical curves. Here, the two superimposed helices may have different handedness and, depending on the geometry of the helices, will rotate either clockwise or counterclockwise when pulled through a fluid. In Fig. 3, it is clear that for larger R , the aggregates, like superhelices, possess a secondary twist of opposite handedness as compared to the geometric expression that describes the position and orientation of one doublet relative to its neighbor. This twist, here left-handed, may be described by the curve

$$\begin{aligned} \mathbf{R}_{twist}(z) = & a(B \cos[(2\pi - 3\alpha)z/(3Z)], \\ & -B \sin[(2\pi - 3\alpha)z/(3Z), z]. \end{aligned} \quad (30)$$

with $\alpha > 0$. This expression is derived by relating the position of the large bead of doublet n_d with the position of the large bead in doublet n_d+3 . Similar expressions that relate the large beads of doublets n_d+1 and n_d+2 with those of n_d+4 and n_d+5 can be obtained by rotating Eq. (30) about the z axis by α and 2α , as well as shifting the z coordinate by the amount Z and $2Z$, respectively. The pitch and wavelength of this helix is much larger than that associated with Eq. (12) (Fig. 5) and therefore, we see that at low N_d the helix described by Eq. (12) dominates. At large values of N_d , however, the clockwise twist is well established and determines the overall handedness of the cluster.

IV. CONCLUSION AND DISCUSSION

In this study, we explored the geometric and hydrodynamic properties of chiral clusters formed by rigid doublets

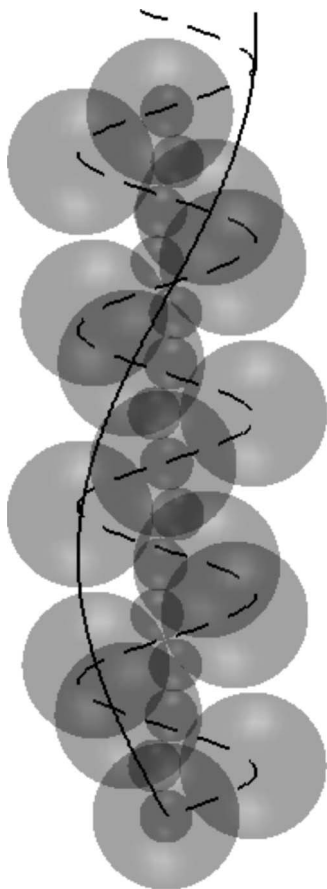


FIG. 5. A cluster with $R=2.75$ and $N_d=15$. The dashed line shows the right-handed helix provided by Eq. (12), while the solid line indicates the superimposed left-handed twist of longer wavelength described by Eq. (30).

composed of two spheres of different radii. We established parametrized helical curves that describe the positions of the beads within each cluster. The parameters governing the pitch and distance from the axis of symmetry depend exclusively on the particle size ratio, R , of the doublet. With the cluster geometry established, we employed FCM to solve two hydrodynamic resistance problems for the collection of spherical particles allowing us to determine entries of the

mobility matrix for the entire cluster. In doing this analysis, we established that clusters composed of doublets with larger R and with higher values of N_d will have a hydrodynamic handedness that is opposite to that of the right-handed parametrized curve providing the geometry. We related this behavior to the left-handed curves of longer wavelength that may also be used to determine the positions of the beads in the aggregates. These curves dominate the hydrodynamic response at large R once established (N_d large).

This study is the first step toward understanding how these aggregates might be used for transport and separation in microfluidic devices. While we have established the direction the aggregates will translate if subject to an applied torque about the helical axis, we have not specified how such a torque might be generated. We are currently investigating the possibility of using time-dependent magnetic or electric fields to generate this torque on cluster. Developing such strategies relies on an appropriate description of the distribution of the magnetic material joining the beads as well as the dielectric properties of the beads themselves. Along with determining effective actuation strategies, classifying the behavior of a suspension of clusters is also of interest. Recent experiments [22] and theoretical [23–26] studies have demonstrated the presence of long wavelength instabilities in suspensions of self-propelled particles which lead to the formation of jets and vortices of length scales much greater than the individual particles. Understanding if such hydrodynamic instabilities will be present in cluster suspensions and quantifying the stabilizing effects of the applied field are essential to the creation of microfluidic transport and separation devices based on these aggregates. As with interacting artificial microswimmers [27], the intercluster magnetic interactions will also affect the performance of such a device and need to be understood as well.

ACKNOWLEDGMENTS

This work was supported by the Applied Mathematical Sciences Program of the U.S. Department of Energy under Contract No. DEFG0200ER25053 and the National Science Foundation under Grant No. 0700669. We also thank the MRSEC center at New York University.

-
- [1] D. Klingenberg, *AIChE J.* **47**, 246 (2001).
 - [2] J. Promislow, A. Gast, and M. Fermigier, *J. Chem. Phys.* **102**, 5492 (1995).
 - [3] E. Climent, M. Maxey, and G. Karniadakis, *Langmuir* **20**, 507 (2004).
 - [4] P. Doyle, J. Bibette, A. Bancaud, and J.-L. Viovy, *Science* **295**, 2237 (2002).
 - [5] S. Bleil, D. Marr, and C. Bechinger, *Appl. Phys. Lett.* **88**, 263515 (2006).
 - [6] A. Rida and M. Gijs, *Anal. Chem.* **76**, 6239 (2004).
 - [7] C. Goubault, P. Jop, M. Fermigier, J. Baudry, E. Bertrand, and J. Bibette, *Phys. Rev. Lett.* **91**, 260802 (2003).
 - [8] S. L. Biswal and A. P. Gast, *Phys. Rev. E* **68**, 021402 (2003).
 - [9] S. Biswal and A. Gast, *Anal. Chem.* **76**, 6448 (2004).
 - [10] R. Dreyfus, J. Baudry, M. L. Roper, M. Fermigier, H. Stone, and J. Bibette, *Nature (London)* **437**, 862 (2005).
 - [11] E. Gauger and H. Stark, *Phys. Rev. E* **74**, 021907 (2006).
 - [12] M. Roper, R. Dreyfus, J. Baudry, M. Fermigier, J. Bibette, and H. A. Stone, *Proc. R. Soc. London, Ser. A* **464**, 877 (2008).
 - [13] E. E. Keaveny and M. R. Maxey, *J. Fluid Mech.* **598**, 293-319 (2008).
 - [14] D. Zerrouki, J. Baudry, D. Pine, P. Chaikin, and J. Bibette, *Nature (London)* **455**, 380 (2008).
 - [15] H. Berg, *Nature (London)* **245**, 380 (1973).

- [16] E. Purcell, Am. J. Phys. **45**, 3 (1977).
- [17] M. Maxey and B. Patel, Int. J. Multiphase Flow **27**, 1603 (2001).
- [18] S. Lomholt and M. Maxey, J. Comput. Phys. **184**, 381 (2003).
- [19] S. Jung, K. Mareck, L. Fauci, and M. Shelley, Phys. Fluids **19**, 103105 (2007).
- [20] J. Stratton, *Electromagnetic Theory* (McGraw-Hill, New York, 1941).
- [21] J. Jackson, *Classical Electrodynamics*, 3rd ed. (Wiley, New York, 1999).
- [22] C. Dombrowski, L. Cisneros, S. Chatkaew, R. E. Goldstein, and J. O. Kessler, Phys. Rev. Lett. **93**, 098103 (2004).
- [23] R. A. Simha and S. Ramaswamy, Phys. Rev. Lett. **89**, 058101 (2002).
- [24] J. P. Hernandez-Ortiz, C. G. Stoltz, and M. D. Graham, Phys. Rev. Lett. **95**, 204501 (2005).
- [25] D. Saintillan and M. J. Shelley, Phys. Rev. Lett. **99**, 058102 (2007).
- [26] D. Saintillan and M. Shelley, Phys. Fluids **20**, 123304 (2008).
- [27] E. E. Keaveny and M. R. Maxey, Phys. Rev. E **77**, 041910 (2008).